Reference number assigned by RILEM: MS

Predicting the flexural load-deflection response of steel fibre reinforced concrete from strain, crack-width, fibre pull-out and distribution data

Authors: P.A.Jones[1], S.A. Austin[2] and P.J.Robins[1]

(1) Dept of Civil & Building Engineering, Loughborough University, UK

(2) Dept of Civil & Building Engineering, Loughborough University, LE11 3TU, UK; email:s.a.austin@lboro.ac.uk; Tel: +44 (0)1509 222608; Fax: +44 (0)1509 223945

ABSTRACT

A semi-analytical model is presented, based on conventional principles of mechanics, to predict the flexure behaviour of steel fibre reinforced concrete. The model uses a stress-block approach to represent the stresses that develop at a cracked section by three discrete stress zones: (a) a compressive zone; (b) an uncracked tensile zone; and (c) a cracked tensile zone. It is further shown that the stress-block, and hence flexural behaviour, is a function of five principal parameters: compressive stress-strain relation; tensile stress-strain relation; fibre pull-out behaviour; the number and distribution of fibres across the cracked section in terms of their positions, orientations and embedment lengths; and the strain/crack-width profile in relation to the deflection of the beam. An experimental investigation was undertaken on both cast and sprayed specimens to obtain relationships for use in the model. The results of the study showed a reasonable agreement between the model predictions and experimental results. However, the accuracy of the model is probably unacceptable for it to be currently used in design. A subsequent analysis highlighted the single fibre pull-out test and the sensitivity of the strain analysis tests as being the main cause of the discrepancies.

1 Introduction

Steel fibre reinforced concrete (SFRC) continues to grow in specialist applications that can utilise its flexibility and enhanced toughness performance, notably sprayed concrete and industrial floors. However, its continued development has been hindered by a general lack of confidence in its design, particularly under flexural load. This is mainly due to a lack of suitable analytical design methods and appropriate material property tests that measure flexural toughness (or strength) parameters. This need is highlighted by the recent RILEM TC162-TDF [1] proposals for test and design methods.

Although recent developments in flexural toughness characterisation have attempted to address the latter of these shortcomings, flexural behaviour of SFRC will be better understood, and thereby predicted, if crack formation and the associated fibre reinforcing mechanisms at the critical section can be explicitly considered in terms of the strain distribution, crack-width and deflection of the beam. To this end, the stress-profile concept potentially offers the most acceptable flexural modelling approach because it is simple to understand; uses conventional principles of structural mechanics, and could, therefore, be incorporated into a design rationale similar to that used for conventional reinforced concrete.

A variety of stress-profile models have been proposed for predicting the load-deflection behaviour of SFRC by utilising the equilibrium of forces at the cracked section [2-5]. These models have generally adopted a semi-analytical approach, whereby failure is assumed to occur at a single crack with rigid-body motion of the two broken halves, rotating about a plastic hinge, being the dominant mechanism.

The kinematics of failure has been modelled using a variety of structural and fracture mechanics theories to relate crack-mouth-opening-displacement (CMOD) to mid-span deflection and the position of the neutral axis. Some authors have simplified the crack profile by assuming that the crack originates at the neutral axis (i.e. CMOD=0) [2-3]. While others have suggested a *fictitious* crack exists close to the neutral axis, whereby cracking is initiated only after the concrete tensile strength is first reached. Tensile strain-softening, according to a stress/crack-width relationship (σ-w), then occurs until the critical crack width is reached (at around 0.05 mm) at which point the *real* crack develops (i.e. σ=0) [5-7].

Under compression, the concrete is assumed to behave according to a parabolic stress-strain relationship, similar to those defined in most design codes [2-3]. However, because there is no single relationship between stress and strain in the cracked region, a variety of approaches have been used to model tensile stress. These have included the use of single fibre pull-out tests in combination with fibre distribution data [3], and theoretical [3, 6, 7] and experimental strain-softening relationships obtained from uniaxial tensile tests [2, 5].

Although all the above mentioned work has helped to extend our understanding of SFRC, the stress-profile models developed to date have used either an assumed stress-block, or an assumed strain profile from which the stress-block is obtained. No attempt has yet been made to ascertain the actual stress-block from strain distributions measured during a flexural beam test. Furthermore, fibre pull-out, fibre numbers and distributions existing at a cracked section have not been explicitly related to the response of the beam under investigation. This may be because no experimental data exists for these parameters, or that current test methods – primarily based on uniaxial tensile testing - are inappropriate for representing the actual behaviour of an SFRC matrix in flexure. Consequently, the stress-profile models currently available cannot fully explain why a certain failure occurs or what the actual fibre contribution is to post-crack flexural performance.

This paper presents work undertaken to investigate the reinforcing mechanisms and fracture processes associated with SFRC under flexural load, in order to develop an alternative stress-profile model to predict flexural behaviour in the form of a load-deflection response using strain, crack-width and fibre pull-out data as the principal modelling parameters. The work formed the final stage of a larger research project investigating sprayed and cast SFRC under flexural load [8-12].

If such a model can be shown to predict reasonably the load-deflection response of SFRC, it could form the basis of a design rationale for predicting flexural behaviour of the material, and thereby provide a much needed link between structural design and flexural toughness performance.

2 Model concepts

The model centres on predicting the stress-profile diagram at the critical section of a SFRC beam in flexure, for a given mid-span deflection. If the shape and magnitude of the stress-profile diagram can be ascertained then it can be used to estimate the flexural capacity of the beam in a similar way that stress-block diagrams are used in conventional reinforced concrete design. Thus, flexural loads can be calculated for any given beam deflection and the complete load-deflection response determined.

The concept of the model is illustrated in Fig. 1, which shows an idealised representation of a crack at the critical section of a SFRC beam, together with the corresponding stress-profile diagram. Using this concept, the concrete stresses and resultant fibre pull-out forces that develop at the critical section can be represented by three distinct zones: (1) compression zone; (2) an uncracked tension zone; and (3) a cracked tension zone. Where the cracked tension zone can be further represented by three sub-zones: an *aggregate bridging zone* - resulting from matrix microcracking which initiates fibre-matrix debonding; a *fibre bridging zone* - in which the fibres are partially pulled out from the matrix; and a *traction free zone* - in which the fibres are completely pulled out from the matrix.

By considering the forces across the critical section in this way the flexural capacity of the critical section can be related to the following five principal parameters:

- the uniaxial compressive stress-strain relationship;
- the uniaxial tensile stress-strain relationship;
- the single fibre pull-out load versus crack-width relationship;
- the number, distribution, embedment lengths and orientations of the fibres bridging the cracked section;
- the strain and crack-width profiles of the uncracked and cracked sections respectively, in relation to the mid-span beam deflection.

If relationships for these parameters can be established, then the shape and magnitude of the stress-block diagram can be predicted for a given beam deflection. Thus, providing the internal force equilibrium of the section is satisfied, the flexural moment capacity of the beam can be computed for a given beam deflection, as follows.

The equilibrium of internal forces is satisfied if the total resultant compressive forces (F_{comp}) and tensile forces ($F_{tensile}$) are equal or, in terms of the individual components of the stress-block diagram

$$\int_0^c \sigma_c (b.dy) + \int_{c'-c}^{c'} \sigma_t (b.dy) + \sum_1^N f_N = 0 \qquad \text{Eq. 1}$$

where σ_c and σ_t are the compressive and tensile stresses respectively, b is the width of the beam, and f_N is the force carried by each of the N individual fibres bridging the cracked tensile zone, as illustrated in Fig. 2. As discussed in 4.3.2 the second term includes the aggregate bridging zone contribution to bending capacity.

The internal moment capacity M_e of the section is computed by summing all the moments generated by the concrete stresses and the individual fibre pull-out forces, multiplied by their position relative to the neutral axis

$$\int_0^c \sigma_c (b.dy).y_c + \int_{c'-c}^{c'} \sigma_t (b.dy).y_t + \sum_1^N (f_N.y_N) = M_e \qquad \text{Eq. 2}$$

where y_c, y_t and y_N are the respective lever arms of the individual forces relative to the neutral axis (Fig. 2).

The flexural load capacity P is obtained by equating the externally applied moment to the internal moment capacity of the section. For a beam tested in third-point loading over a span l, this equates to

$$P = \frac{6M_e}{l} \qquad \text{Eq. 3}$$

By repeating this process for various mid-span beam deflections, the flexural load-deflection response can be determined for the given beam under investigation.

When assessing the flexural capacity of a SFRC beam using this approach, the following assumptions are made:

- failure occurs at a single crack within the middle third of a four-point loaded beam, and shearing and strain effects are negligible;
- the stresses and forces in compression and tension are as shown in Fig. 1;
- the stresses and pull-out forces acting across the critical section are purely uniaxial;
- the beam is of homogenous material and is elastically isotropic; and
- plane cross-sections remain plane.

3 Experimental programme

3.1 Overview

An experimental investigation was undertaken, using a typical wet process steel fibre reinforced sprayed concrete mix design, to obtain the necessary data to implement and verify the model. Four experimental tests were developed to determine relationships for the principal modelling parameters. In addition, a programme of standard flexural toughness beam tests was undertaken to establish typical load-deflection curves against which the model results could be compared.

3.2 Materials and mix proportions

The constituent materials of the SFRC mix used in the investigation were typical of those used in wet process steel fibre reinforced sprayed concrete. The cement was Class 42.5N Portland Cement (PC) conforming to BS12 [13], the condensed silica fume was a 50% water based slurry, the aggregate was a 6 mm maximum sized uncrushed river gravel generally conforming to the grading limits of the EFNARC [14], the superplasticiser was a melamine-formaldehyde and the steel fibres were of the hooked end type (30 mm long, 0.5 mm diameter and collated).

The base concrete mix had a water: cementitious:aggregate ratio of 0.45:1.0:2.8, and contained silica fume replacement at 10% by weight of cement. Steel fibres were added to the base mix in quantities of 40 and 80 kg/m^3 (0.5 and 1.0 % by volume respectively). The base concrete developed a 28-day compressive strength of 72 MPa, (determined from 100 mm cubes) and the mix design and testing age were kept constant throughout the testing programme.

The majority of the test programme used cast (as opposed to sprayed) specimens so that the test variables and material parameters under investigation could be better controlled. However, specimens for the strain analysis, fibre distribution and flexural toughness beam tests were also obtained from spraying trials undertaken by an experienced contractor on the site of a wet process SFRC project. The sprayed base mix was the same as the cast mix, except that the in situ fibre contents were 26 and 66 kg/m^3 (0.34 and 0.87 % by volume respectively).

3.3 Strain/crack-width analysis tests

A strain analysis technique, which combines the use of electrical resistance strain gauges (5-8 per beam – depending on depth – with one fixed to the compressive face and the others evenly distributed down the side of each specimen) with a semi-automated grid method (using digital image processing) was developed to measure the strain and crack-width profile at the critical section of a SFRC beam during a flexural toughness test. The test programme comprised 6 cast and 2 sprayed test series as shown in Table 1. Each test series consisted of two beam specimens. The technique is capable of measuring strain to an accuracy of ± 15 με over a range of 200 με (tension) to 3500 με (compression), and crack-widths greater than 0.2 mm to an accuracy of ± 0.1 mm from the grid method, with the possibility of crack-width information in the range 0-0.1 mm from the strain gauges.

Strain blocks obtained from the strain gauge analysis were combined with crack width profiles obtained from the grid method, in order to determine the complete strain/crack-width profile, at a given mid-span deflection, for use in the model. Table 2 provides an overall summary of the strain/crack-width test data that was used in the model analysis.

Further details about the test procedure and discussion of results can be found in reference 9.

3.4 Single fibre pull-out tests

A single fibre pull-out test was developed, to enable the fibre pull-out response to be measured for a range of fibre embedment lengths and orientations. The test programme comprised 21 test series involving 3 fibre embedment length (5, 10 and 15mm) and 7 fibre orientation (0, 10, 20, 30, 40, 50 and 60 degrees) combinations with 4 samples in each test series. The results were used, in combination with the fibre distribution data, to model and analyse the forces transferred by the fibres bridging the cracked tensile zone (Fig. 1).

Further details about the test procedure and discussion of results can be found in reference 10.

3.5 Fibre distribution analysis

Two experimental techniques were developed to obtain the necessary fibre distribution data for use in the model.

The first was an X-ray photographic analysis to determine the probability distribution associated with fibre embedment length and fibre orientation occurring across a cracked beam section. The test programme involved 75 mm deep beam specimens and comprised 2 cast test series (at fibre volumes of 40 and 80 kg/m^3) and 2 sprayed test series (at fibre volumes of 26 and 66 kg/m^3) with 2 samples in each test series. Table 3 provides a summary of the probability distributions obtained from the tests.

The second was a manual fibre counting method to measure fibre density distribution occurring at the cracked section of a beam specimen following a flexural toughness test. The test programme comprised 6 cast test series and 2 sprayed test series with 2 samples per test series . Test variables investigated included: fibre volume and beam depth. Table 4 provides a summary of the fibre density distributions obtained from the test.

The results from these tests were used in combination with the single fibre pull-out data to predict the forces transferred by the fibres bridging the cracked tensile zone in the model analysis.

Further details about the test procedure and discussion of results can be found in reference 11.

3.6 Compression tests

A compression test was developed based on the recommendations of BS188: part 121 [15] to measure the uniaxial compressive stress-strain responses and secant modulus for a range of fibre volume contents used in the research. The test used prism specimens measuring 76 x 76 x 229 mm. The test programme comprised 3 cast test series (at fibre volumes of 0, 40 and 80 kg/m^3) and 2 sprayed test series (at fibre volumes of 26 and 66 kg/m^3).

The results, in the form of stress-strain response curves, were used in combination with the strain analysis test data to determine the compressive stress-block diagram for use in the model. Average values for peak compressive stress, strain at peak stress and compressive secant modulus, for the matrix used in the investigation, were 65 MPa (SD 1.8), 2815 με (SD 58) and 33 GPa (SD 0.9) respectively. It was found that the matrix compressive properties were generally not influenced by fibre content up to 80 kg/m^3 . The results indicated no significant difference between the compressive behaviour of the cast and sprayed specimens used in the investigation. The coefficient of variation varied between 1-4% for the cast specimens and between 2-5% for the sprayed specimens.

Further details about the test procedure and analysis of the results can be found in reference 12.

3.7 Flexural toughness beam tests

A programme of flexural toughness tests was also undertaken to establish a set of load-deflection curves against which the model could be compared and verified.

The test programme comprised 6 cast and 2 sprayed test series and mirrored the strain analysis test programme summarised in Table 1. Each test series consisted of three beam specimens.

Specimens were tested over a span of 450 mm in third-point loading using a 100 kN capacity floor-mounted Instron 6025 testing machine. Average mid-span beam deflections were measured using two LVDTs mounted on a yoke around the specimen to enable net mid-span deflections to be recorded. Tests were performed under closed-loop deflection control using net mid-span beam deflection.

4 Model development

4.1 Compression zone

The compressive stress-block was determined by applying the experimentally obtained compressive stress-strain response curves directly to the compressive strain-block, for each mid-span beam deflection under consideration.

4.2 Uncracked tensile zone

The uncracked tensile stress-block was determined by applying a linear elastic tensile stress-strain relationship directly to the uncracked tensile strain block determined from the strain analysis tests and compressive secant modulus data determined from the compression tests, at each mid-span deflection considered. This approach was based on the assumptions that the beam is of a homogenous material (i.e. has the same value of Young's modulus in both compression and tension), and the tensile stress-strain relationship is linear up to the matrix cracking strain of 190 με (this being the average cracking strain determined from the strain analysis tests).

4.3 Cracked tensile zone

4.3.1 Probabilistic fibre pull-out curve

In Fig. 1 the cracked tensile zone is shown to consist of three sub-zones: an aggregate bridging zone, a fibre bridging zone and a traction free zone. The forces transferred across the cracked tensile zone are primarily dependent on the pull-out behaviour of individual fibres bridging the crack. In the model these forces are modelled using single fibre pull-out test data in combination with fibre distribution data (i.e. fibre embedment lengths and orientations) measured across the crack. However, in order to use this approach two key data sets were required: (a) the number and position of the individual fibres bridging the cracked section; and (b) the fibre embedment length and fibre orientation of each fibre bridging the cracked section.

The first of these was obtained by using the results from the manual fibre counting analysis to provide data relating to both the number and distribution of fibres bridging the cracked section of each beam (Table 4). However, because it is not possible to apply a separate pull-out response curve to every fibre bridging the cracked section, an alternative approach (based on a probability analysis) was developed to combine statistically all the single fibre pull-out test responses (that is, for all the different combinations of fibre embedment length l_f and fibre orientation θ_f) into a single pull-out response curve. This curve, hereafter termed the *probabilistic fibre pull-out curve*, represents the most probable pull-out response of each fibre bridging the cracked section.

The probabilistic fibre pull-out curve was determined from the experimental test data as follows:

(a) The results of the X-ray analysis (Table 3) were used to determine the combined probability of each combination of l_f and θ_f occurring at any location of the cracked section.

(b) Average fibre pull-out loads were then determined from the single fibre pull-out test responses, in increments of 0.05 mm (up to a crack width of 5 mm), for each combination of l_f and θ_f investigated.

(c) For each combination of l_f and θ_f, the average fibre pull-out loads were multiplied by their probability of occurrence to obtain weighted fibre pull-out loads. These weighted loads were then summed together to obtain a total 'probabilistic' fibre pull-out load for each crack-width, increment of 0.05 mm.

(d) Finally, the probabilistic fibre pull-out loads were plotted against the corresponding crack-widths.

The resulting probabilistic fibre pull-out curve is shown in Fig. 3, together with the corresponding curve determined by assuming a random fibre distribution (i.e. assuming all the combinations of l_f and θ_f have an equal probability of occurrence). A significant difference in the magnitude of these curves can be seen, particularly up to a crack-width of 2 mm where the loads associated with the random distribution curve are up to 40% lower than the actual curve used in the model. The greater pull-out loads associated with the actual curve are the result of the measured fibre distribution being skewed towards fibre orientations between 0-30 degrees (Table 3) as a result of confinement effects imposed on the fibres during preparation of the beam specimens [11].

4.3.2 Aggregate bridging zone

Due to the relative difficulty associated with the experimental determination of the strain softening behaviour of plain and SFRC concrete, a semi-theoretical strain softening relationship (σ–w curve) was derived, for use in the model up to a crack-width of 0.05 mm, using the law of mixtures. This was achieved by combining a theoretical tensile σ–w curve for the plain concrete matrix with the probabilistic fibre pull-out curve (Fig. 3) converted to stress.

The tensile stress in the plain concrete under strain-softening (σ_{ct}) was taken to decrease exponentially, according to the relationship reported by Gopalaratnam and Shah [16]:

$$\sigma_{ct} = \sigma_{t(\max)} \cdot e^{-k \cdot w \cdot \lambda} \qquad \text{Eq. 4}$$

where $\sigma_{t(max)}$ is peak tensile stress (MPa) and k and λ are empirical shape constants, and w is the crack width (mm).

A value of fibre pre-stress was also included in the determination of the resulting σ–w curve, which was taken to be the stress in the fibres at the instant the matrix cracks. For the 0.5 mm diameter fibres used in the experimental investigation, assuming a Young's modulus of 205 GP and a matrix cracking strain of 190 με, equated to a fibre pre-stress of 40 MPa.

Fig. 4 shows the resulting σ–w curves for fibre volumes of 0.5 and 1.0% (40 and 80kg/m^3 respectively) using values of 1.0 and 60.8 for the empirical constants λ and k respectively as recommended by reference 16. Similar curves were determined for the sprayed specimens. The curves were used to determine the aggregate bridging stress-block for each mid-span deflection considered by applying them directly to the crack-width profiles determined from the strain analysis tests. By using this approach, the boundary between the aggregate bridging zone (modelled using a stress versus crack- width relationship) and the fibre bridging zone (modelled using a fibre pull-out load versus crack-width relationship) was found to occur at a crack-width of approximately 0.05mm.

4.3.3 Fibre bridging zone

The fibre bridging forces were determined by relating the probabilistic fibre pull-out curve (Fig. 3) to the crack-width profile at each mid-span deflection considered, and then combining the resulting single fibre pull-out loads with the fibre density data obtained from the manual fibre counting analysis described previously (Table 4).

The fibre bridging zone was first divided into equal sized layers, termed *fibre* zones, as used in the manual fibre counting analysis (Table 4). The average crack-widths, measured at the mid-point of each fibre zone, were determined by superimposing the appropriate crack-width profile onto the fibre zone layout. The single fibre pull-out force P_n associated with each fibre zone could then be determined by relating the probabilistic fibre pull-out curve to each value of crack-width. The total fibre pull-out force F_n transferred across the crack by each fibre zone was determined by multiplying the values of P_n by the total number of fibres occurring in each fibre zone:

$$F_n = P_n \,.(N_f)_n \,.\, b \qquad \text{Eq. 5}$$

where $(N_f)_n$ is the fibre density (measured as fibres/cm^2) associated with each fibre zone and b is the width of the beam.

4.3.4 Traction free zone

Theoretically, the boundary between the traction free zone and the fibre bridging zone occurs at a crack-width of 15mm (that is, a crack-width corresponding to half the length of a 30mm long fibre). It is only then that all the fibres will have been completely pulled-out, and no force will be transferred across the cracked section. However, the crack-widths associated with the test beams investigated here never exceeded 5mm, and so the traction free zone did not develop. Therefore, it is not considered in the model analysis presented here.

5 Implementation

The implementation of the model is based on establishing five principal points associated with the strain/crack-width profiles, which provide the boundaries between the various stress zones. These are the points of (Fig. 1): maximum compressive strain; neutral axis; zero crack-width; zero matrix tensile stress; and CMOD. Once these points have been established for a given mid-span deflection, then the remaining model data can be applied to determine stresses and forces, and thus flexural moment capacity at the critical section can be calculated once equilibrium of the section is satisfied.

A spreadsheet was developed (in MS Excel) to run the model analysis and determine the load/deflection response for each of the beam type/fibre volume combinations considered. For each beam analysed, flexural loads were predicted at mid-span deflections of 0.1, 0.2, 0.5, 1.0 2.0 and 4.0mm.

The experimentally determined strain and crack-width profiles were applied directly to the model. The experimental design allowed the resulting NA depths to be verified by checking for equilibrium of the calculated forces (i.e. there was redundant information). This showed generally good agreement (i.e. a difference of 0-10% in depth of the beam) but inevitably the neutral axis depth measured from the strain gauges always had to be altered slightly in order to satisfy equilibrium of the internal forces at the section under investigation. Therefore, the final model analysis used only measured values of the maximum compressive strain and the corresponding CMOD (Table 2), (i.e. excluding the intermediate strain gauges values and grid measurements) the position of the neutral axis being determined , by trial and error, until equilibrium of the internal forces was satisfied. In general, calculated neutral axis depths were between 0-5mm nearer the compressive face of the beam than measured depths. However, for deflections at 0.2mm and 0.5mm the calculated depths were up to 10mm closer to the compressive face than measured depths.

6 Results and discussion

Comparisons between the predicted load-deflection responses, derived from the model, and those obtained experimentally from the flexural toughness beam tests for a selection of the beams investigated are shown in Figs. 5-8. It can be seen from theses plots that although the model appears to predict the general shape of the load-deflection response, the accuracy of the predictions are generally poor and highly variable. This is shown in Table 5, which summarises the average differences for the eight test series analysed in terms of mean and standard deviation of load and neutral axis position at each mid-span deflection. The results show that the model predicts the portion of the load-deflection response up to a deflection of 0.2 mm reasonably well, but loads between 0.5-1.0 mm deflection are generally underestimated and loads between 2.0-4.0 mm are generally overestimated. In contrast, as described above, the model appears to predict the position of the neutral axis reasonably well, indicating the suitability of the strain/crack-width profiles obtained experimentally.

In an attempt to improve the performance of the model, further analysis was undertaken to determine the causes of the discrepancies and thereby improve its accuracy.

Given that the loads in the uncracked region of the load-deflection response (up to a deflection of 0.1mm) were generally predicted to within 20% of the their measured values, it appears that the uncracked compressive and tensile stress zones were modelled reasonably well by the experimental data. Thus, the strain profiles (which were shown to be within 15 με of their theoretical values) and the measured compressive stress-strain relationships appear to be appropriate for use in the model. Furthermore, because the number and distribution of the fibres were obtained by analysing the actual cracked section of the beams under investigation, it is unlikely that this data adversely affected the model predictions. Thus, the model deficiencies appear to be caused by either: (i) the crack-width profiles; and (ii) the probabilistic fibre pull-out curve, determined from the single fibre-pull-out test results; or a combination of the two mechanisms.

In terms of the crack-width profiles, it was shown previously that the grid method is suitable for measuring crack-widths greater than 0.2 mm to an accuracy of ± 0.1 mm. Therefore, in order to investigate the effect of inaccuracies in crack-width measurements on the model predictions, an additional sensitivity analysis was undertaken on the data by altering the measured CMOD values by an amount equivalent to the accuracy of the grid method (that is, by $\pm$ 0.1mm). The results showed that a reduction of 0.1 mm in the CMOD at a deflection of 0.2mm increased the value of the predicted load, to an extent that they compare favourably with the measured loads. However, an increase in CMOD by the same amount had virtually no effect. Similarly, there was virtually no effect on the predicted loads due to an increase or decrease in the measured CMOD by ± 0.1 mm at deflections greater than 0.2 mm. Given that the measured CMOD values at a 0.2 mm deflection were less than 0.2mm for all the beams analysed (Table 4), it appears that the limitations of the grid method (in terms of its accuracy and sensitivity) will only have a significant effect on the model predictions in the deflection range between 0.1-0.2 mm.

From the foregoing discussions, it appears that the probabilistic fibre pull-out curve is causing the main discrepancies associated with the model predictions between mid-span deflections of 0.5-4.0mm. In particular, the results shown in Fig. 5-8 indicate that the shape and magnitude of this curve may be inappropriate for use in the model. Therefore, a sub-analysis was undertaken on the shape and magnitude of the probabilistic fibre pull-out curve, by comparing it with similar curves published elsewhere in the literature. The results of this analysis are shown in Fig. 9 which compares the probabilistic curves shown in Fig. 3 with similar curves obtained from single fibre pull-out tests by Armelin and Banthia [3] and an inferred single fibre pull-out response, determined from a related study [17], using back analysis from the load-deflection responses of seven beams from series 75C(40), four of which are shown in Fig 6.

In respect of the work of Armelin and Banthia [3] they adopted a similar approach to that described herein to determine their average single fibre pull-out curve, except that they assumed a random 3-D fibre distribution and incorporated a separate contribution for the strength of the fibre hook. However, it is not clear how the shape and magnitude of the contribution of the hook was determined. Thus, for comparative purposes both the curves with and without the contribution of the hook are shown in Fig. 9.

The curves shown in Fig. 9 indicate some very significant differences. In particular, the crack-width at peak load of the probabilistic fibre pull-out curve (occurring at around 1.2 mm) is very different from that suggested by Prudencio *et* al [17] and Armelin and Banthia [3], where peak load occurs at around 0.1 mm. In addition, the general shape of the probabilistic curve is very different from the other author's curves. In contrast, the peak load of the probabilistic curve (occurring at around 135 N) compares very well with both the other author's curves. Furthermore, the shape and magnitude of the random 3-D probabilistic curve compares very well with Armelin and Banthia's curve (also based on random 3-D fibre orientation) without the contribution of the hook.

These results suggest that the fibre pull-out response obtained from single fibre pull-out tests in uniaxial tension may not be representative of the pull-out behaviour of fibres in a beam specimen under flexure. Therefore, in order to test this hypothesis, the model analysis was repeated for each of the other seven beam series using the inferred pull-out curve shown in Figs. 9. A summary of the results, comparing model predictions with measured load values, are given in Table 6 and 7, together with the individual load-deflection responses for each beam in Fig. 10-16. The results show a much improved agreement between the predicted and measured load data, with the load generally being predicted to within 10-20% of the measured values for all seven beam series and neutral axis depths being predicted to within 3mm of measured values. In addition, the shape of the predicted load-deflection curves is much closer aligned to the measured responses, particularly at lower deflections.

These results provide evidence that the single fibre pull-out test (undertaken in uniaxial tension) is not representative of the behaviour of fibres pulling out of a concrete matrix in flexure, and that the resulting response significantly overestimates the deflection at peak pull-out load, which in turn means that the resulting pull-out response curve is unrepresentative of actual behaviour. However, although these results help to better understand the behaviour of single fibres pulling out of a concrete matrix in flexure, the question still remains as to how the actual fibre pull-out response should be determined experimentally.

7 Conclusions

A semi-analytical model has been proposed for predicting the load-deflection response (and hence the flexural toughness performance) of both sprayed and cast steel fibre reinforced concrete beams in flexure. The main merits of the model are (a) the stress block approach which is familiar to all structural engineers designing reinforced concrete; (b) its use of conventional principles of mechanics; (c) its use of principal parameters determined from tests on laboratory specimens; and (d) its potential for incorporating into a design rationale for steel fibre reinforced concrete (SFRC). The main objective has been to establish the feasibility of the approach. From a commercial perspective, the cost of establishing the material

parameters will be important; as with conventionally reinforced concrete, it should be possible to establish many of these generically.

Although the flexural load-deflection responses predicted by the model compared favourably with experimental data, the accuracy of the model is probably unacceptable for it to be currently used in design. A subsequent analysis highlighted the single fibre pull-out test and the sensitivity of the strain analysis tests, adopted in the collection of experimental data for use in the model, as being the main cause of the discrepancies. In particular, it was shown that the results of single fibre-pull out tests – undertaken in direct tension - may not be representative of the behaviour of multiple fibres acting in concrete under flexure, and that improvements in such tests (or use of alternative techniques) are required in order to obtain more representative fibre pull-out verses crack-width response curves.

The research presented here has shown that it is possible to predict the complete load-deflection response of a SFRC beam, from conventional principals of mechanics, providing the following principal parameter relationships are known: the compressive stress/strain relationship; the uncracked tensile stress/strain relationship; the tensile stress/crack-width relationship; the single fibre pull-out response (in respect of fibre pull-out load, orientation, and embedment length); the fibre density distribution across the critical section; and the strain and crack-width profile at the critical section in relation to mid-span beam deflection.

Acknowledgements

The authors are grateful to Gunform Ltd for their assistance with the sprayed concrete field trials.

References

[1] RILEM TC 162-TDF, 'Test and design methods for steel fibre reinforced concrete – uni-axial tension test for steel fibre reinforced concrete', *Materials and Structures* **34** (1) (2001) pp 3-6.

[2] Casanova, P. and Rossi, P., 'Analysis of metallic fibre-reinforced concrete beams submitted to bending', *Materials and Structures*. **29** (1996) 354-361.

[3] Armelin, H.S. and Banthia, N., 'Predicting the flexural postcracking performance of steel fiber reinforced concrete from the pullout of single fibers', *ACI Mater. J.* **94** (1) (1997) 18-31.

[4] RILEM TC 162-TDF, 'Test and design methods for steel fibre reinforced concrete – σ-ε design method', *Materials and Structures* **35** (2002) 262-278.

[5] Ulfkjaer, J., Krek, S., and Brincker, R., 'Analytical model for fictitious crack propagation in concrete beam', *ASCE J. Engineering Mechanics* **121**(1) (1995) 7-15

[6] Hillerborg, A., 'Analysis of fracture by means of the fictitious crack model particularly for fibre reinforced concrete', *Int. J. Cem. Compos*. **2** (4) (1980) 177-184.

[7] Wecharatana, M., and Shah, S.P., 'A model for predicting fracture resistance of fiber reinforced concrete', *Cem. Concr. Res*. **13** (1983) 819-829.

[8] Robins, P.J., Austin, S.A. and Jones, P.A., 'Flexural modelling of steel fibre reinforced sprayed concrete', in 'Sprayed Concrete Technology', Proceedings of the ACI/SCA International Conference on Sprayed Concrete/Shotcrete, Edinburgh, Sept. 1996 (E&FN Spon, London, 1996) 107-114.

[9] Robins, P.J., Austin, S.A., Chandler, J.M. and Jones, P.A., 'Flexural strain and crack-width measurement of steel-fibre-reinforced concrete by optical grid and electrical gauge methods', *Cem. Concr. Res*. **31** (5) (2001) 719-729.

[10] Robins, P.J., Austin, S.A and Jones, P.A., 'Pull-out behaviour of hooked steel fibres', *Materials and Structures*. **35** (2002) 434-442.

[11] Robins, P.J., Austin, S.A and Jones, P.A., 'Spatial distribution of steel fibres in sprayed and cast concrete', *Mag. Concr. Res*. **55** (3) (2003) 225-235.

[12] Jones, P.A., 'Flexural Modelling of Steel Fibre Reinforced Sprayed Concrete', Ph.D Thesis (Loughborough University, England, 1998).

[13] BS 12 (1992) Specification for Portland Cements, British Standards Institution, Milton Keynes.

[14] EFNARC (1996) European Specification for Sprayed Concrete, European Federation of National Association of Specialist Repair Contractors and Material Suppliers for the Construction Industry, Aldershot, UK.

[15] BS 1881: Part 121 (1983) Method of Determination of Static Modulus of Elasticity in Compression, British Standards Institution, Milton Keynes.

[16] Gopalaratnam, V.S. and Shah, S.P., 'Softening response of plain concrete in direct tension', *ACI J.* **82** (1985) 310-323.

[17] Prudencio, L., Austin, S.A., Jones, P.A., Armelin, H.S. and Robins, P.J., 'Prediction of steel fibre reinforced concrete under flexure load from an inferred fibre pull-out response',*Materials and Structures.* **39** (2006) 599-608.

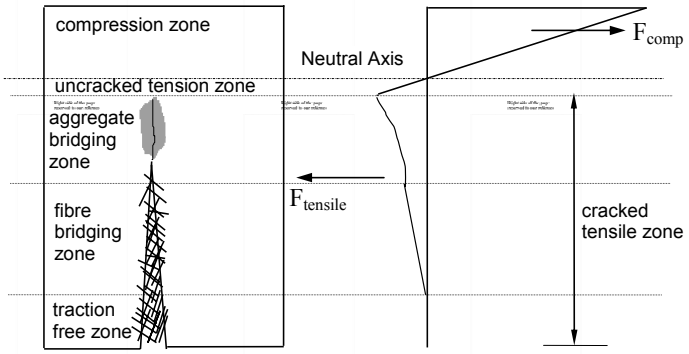

Fig. 1- Schematic representation at the cracked section of steel fibre reinforced concrete beam under flexural loading.

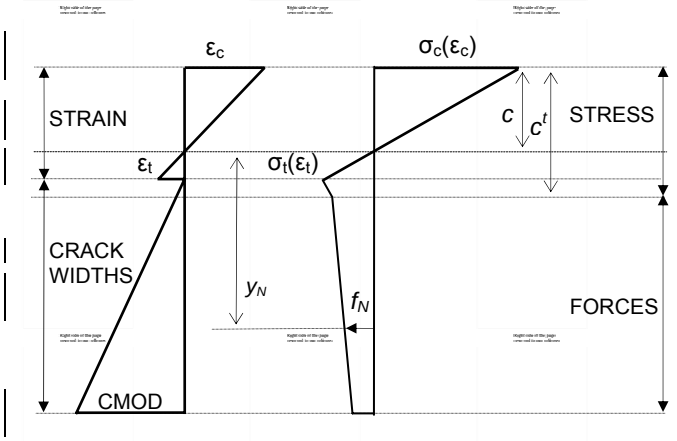

Fig. 2 - Schematic representation of the stress/strain and force/crack-width blocks acting across the cracked section.

Table 1 – Summary of strain analysis test programme

Series ref.	Beam depth (mm)	Beam width (mm)	Beam length (mm)	Fibre content (kg/m^3)	Cast/ sprayed
50C(40)	50	100	500	40	cast
50C(80)	50	100	500	80	cast
75C(40)	75	100	500	40	cast
75C(80)	75	100	500	80	cast
100C(40)	100	100	500	40	cast
100C(80)	100	100	500	80	cast
75S(26)	75	125	500	26	sprayed
75S(66)	75	125	500	26	sprayed

Table 2 – Summary of strain/crack-width data used in model analysis

Series reference		Mid-span deflection (mm)					
		0.1	0.2	0.5	1.0	2.0	4.0
50C(40) & 50C(80	CMOD (mm)	-	0.06	0.20	0.35	0.85	1.65
	εmax (με)	145	280	705	1210	2035	3140
75C(40) & 75C(80	CMOD (mm)	-	0.05	0.25	0.65	1.40	3.00
	εmax (με)	155	530	985	1350	1890	3020
100C(40) & 100C(80	CMOD (mm)	-	0.07	0.25	0.75	1.70	3.65
	εmax (με)	195	410	675	1040	1900	2895
75S(26) & 75S(66)	CMOD (mm)	-	0.05	0.25	0.65	1.40	3.00
	εmax (με)	155	530	985	1350	1890	3020

Table 3 – Fibre probability distributions determined from X-ray analysis

(a) Fibre embedment length, l

Nominal embedment length (mm)	Range represented (mm)	Probability of occurrence
5	$0 \le l < 4.5$	0.267
10	$4.5 \le l < 11.5$	0.466
15	$11.5 \le l \le 15.0$	0.267

(b) Fibre orientation, Θ

Nominal fibre orientations(degrees)	Range represented (degrees)	Probability of occurrence
0	$0 \le \Theta < 10$	0.04
10	$10 \le \Theta < 20$	0.17
20	$20 \le \Theta < 30$	0.21
30	$30 \le \Theta < 40$	0.19
40	$40 \le \Theta < 50$	0.16
50	$50 \le \Theta < 60$	0.10
60	$60 \le \Theta \le 90$	0.13

Table 4 – Summary of fibre densities determined from manual counting anlaysis (fibres/cm^2)

		75C(40)		75C(80)		75S(26)		75S(66)	
Beam depth zone (mm)	Depth to mid-point (mm)	mean	SD	mean	SD	mean	SD	mean	SD
0-5	2.5	1.8	0.6	2.9	1.2	1.0	0.0	3.3	1.6
5-15	10	1.3	0.3	2.0	0.8	0.8	0.6	1.9	0.7
15-25	20	1.2	0.4	1.9	0.6	0.9	0.3	2.1	1.0
25-35	30	1.3	0.6	2.3	0.4	0.9	0.3	2.4	0.4
35-45	40	1.4	0.3	2.5	0.6	1.0	0.1	2.6	0.4
45-55	50	1.2	0.3	2.9	0.4	1.0	0.1	2.1	0.6
55-65	60	1.3	0.3	2.5	0.6	0.8	0.4	2.1	0.2
65-75	70	1.2	0.5	2.4	0.5	0.6	0.4	1.4	0.8
Av.		1.3		2.3		0.9		2.2	
		50C(40)		50C(80)		100C(40)		100C(80)	
0-10	5	1.3	0.1	3.8	0.3	1.1	0.1	1.9	0.4
10-20	15	1.4	0.1	1.9	0.5	1.2	0.6	2.1	0.0
20-30	25	1.3	0.1	2.9	0.8	1.0	0.1	1.5	0.5
30-40	35	1.5	0.8	2.3	1.5	0.6	0.1	1.7	0.1
40-50	45	1.7	0.4	2.6	1.1	0.8	0.6	1.2	0.7
50-60	55					0.8	0.2	2.3	0.2
60-70	65					1.1	0.2	1.8	0.4
70-80	75					1.6	0.9	2.6	0.2
80-90	85					1.5	0.0	2.3	0.1
90-100	95					1.1	0.4	2.5	0.5
Av.		1.4		2.6		1.1		2.0	

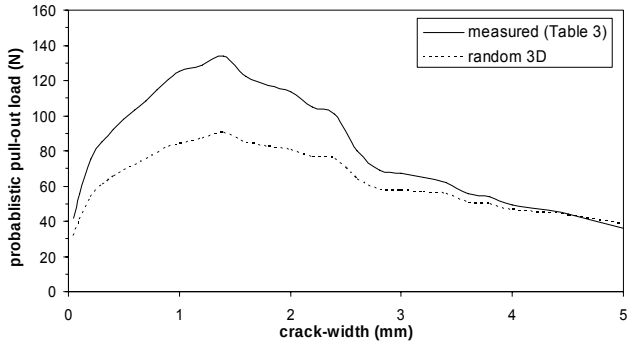

Fig. 3 - Probabilistic single fibre pull-out curve.

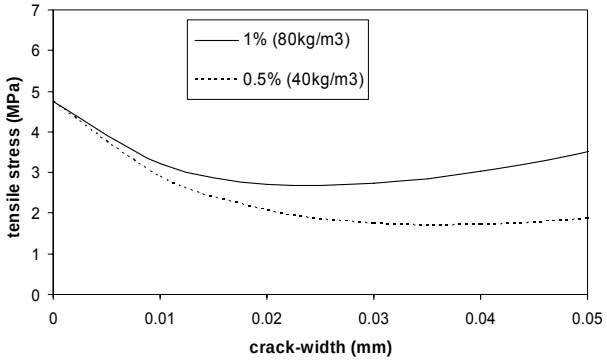

Fig. 4 - Tensile stress versus crack-width (σ–w) curves used in the model analysis.

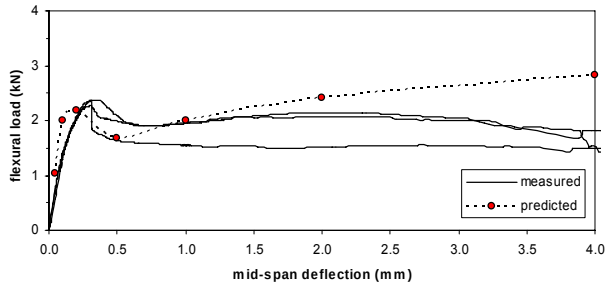

Fig. 5 - Comparison between predicted and measured response – 50 x 100 mm cast beam, 40 kg/m^3 (probabilistic fibre pull-out curve).

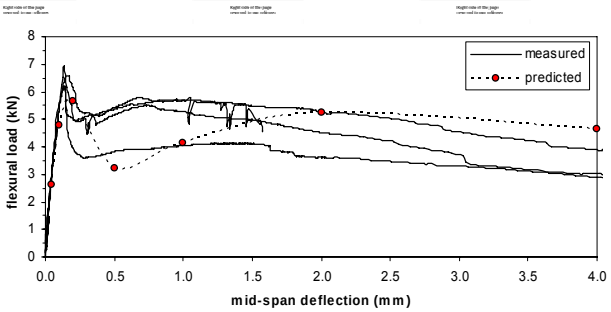

Fig. 6 - Comparison between predicted and measured response – 75 x 100 mm cast beam, 40 kg/m^3 (probabilistic fibre pull-out curve).

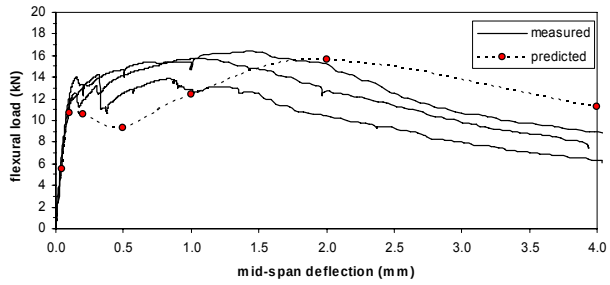

Fig. 7 - Comparison between predicted and measured response – 100 x 100 mm cast beam, 80 kg/m^3 (probabilistic fibre pull-out curve).

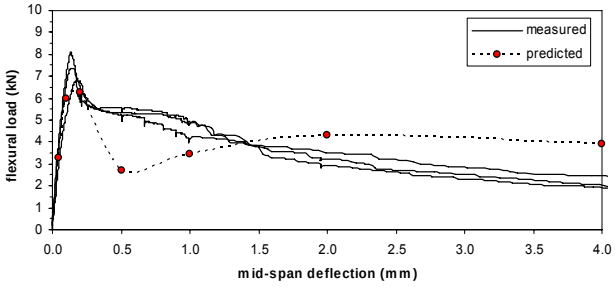

Fig. 8 - Comparison between predicted and measured response – 75 x 125 mm sprayed beam, 26 kg/m^3 (probabilistic fibre pull-out curve).

Table 5 – Summary of differences between predicated and measured load and neutral axis position (using probabilistic fibre pull-out response)				
Deflection (mm)	Load (%)		Neutral axis (mm)	
	Mean	SD.	Mean	SD
0.1	2	21	1.0	0.8
0.2	0	14	-0.1	2.7
0.5	-34	11	-3.3	2.1
1	-18	11	-1.8	2.6
2	17	14	0.6	1.7
4	51	26	1.0	1.4

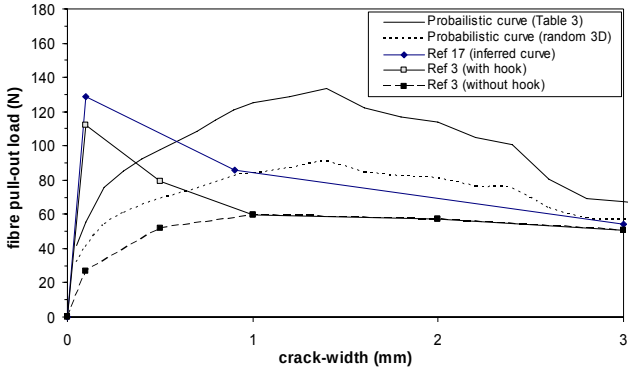

Fig. 9 - Comparison between probabilistic fibre pull-out curves with similar curves reported in literature.

Table 6 – Summary of differences between predicated and measured load and neutral axis position (using inferred fibre pull-out response)				
Deflection (mm)	Load (%)		Neutral axis (mm)	
	Mean	SD.	Mean	SD
0.1	2	21	1.0	0.7
0.2	14	13	2.3	4.5
0.5	6	16	0.1	3.5
1	2	20	-0.6	3.3
2	-3	15	-0.2	2.5
4	7	17	-0.1	1.6

Table 7 – Comparisons between the model predictions and experimental results (using inferred fibre pull-out response)

Series ref.	Mid-span deflection (mm)	Model		Experimental		Differences	
		Load (kN)	NA depth (mm)	Av. Load (kN)	NA depth (mm)	Load (%)	NA depth (mm)
50C(40)	0.1	2.0	25.1	1.6	24.9	24	0.2
	0.2	2.3	18.9	2.2	18.9	7	0.0
	0.5	2.6	8.7	2.1	9.3	25	-0.6
	1.0	2.7	5.6	2.0	4.4	34	1.2
	2.0	2.5	3.5	2.1	3.2	17	0.3
	4.0	1.9	2.5	1.7	2.4	14	0.1
50C(80)	0.1	2.0	25.1	1.4	24.9	42	0.2
	0.2	3.1	22.2	2.3	18.9	36	3.3
	0.5	3.9	12.4	3.3	9.3	17	3.1
	1.0	4.3	8.7	3.4	4.4	27	4.3
	2.0	4.0	5.5	3.8	3.2	6	2.3
	4.0	3.4	4.4	2.9	2.4	17	2.0
75C(80)	0.1	4.8	37.7	5.8	37.0	-18	0.7
	0.2	8.7	23.9	7.0	21.9	24	2.0
	0.5	9.6	14.9	7.9	12.1	21	2.8
	1.0	9.2	11.3	8.4	10.5	9	0.8
	2.0	7.6	7.6	8.1	5.1	-6	2.5
	4.0	6.0	5.1	6.1	3.5	-2	1.6
100C(40)	0.1	10.7	50.3	10.7	48.1	0	2.2
	0.2	9.3	28.7	9.4	22.9	-1	5.8
	0.5	8.7	15.9	10.2	18.9	-14	-3.0
	1.0	7.4	8.7	9.8	12.8	-24	-4.1
	2.0	5.9	4.6	8.8	9.3	-33	-4.7
	4.0	4.4	3.0	6.1	5.7	-27	-2.7
100C(80)	0.1	10.7	50.3	11.0	48.1	-3	2.2
	0.2	12.9	34.8	12.8	22.9	1	11.9
	0.5	14.8	24.4	13.1	18.9	13	5.5
	1.0	13.4	15.0	14.0	12.8	-4	2.2
	2.0	10.9	8.0	12.0	9.3	-9	-1.3
	4.0	8.2	5.3	7.5	5.7	9	-0.4
75S(26)	0.1	6.0	37.7	6.5	37.0	-8	0.7
	0.2	7.1	18.5	6.6	21.9	7	-3.4
	0.5	4.6	7.1	5.5	12.1	-17	-5.0
	1.0	4.2	5.0	4.7	10.5	-11	-5.5
	2.0	3.4	3.1	3.3	5.1	2	-2.0
	4.0	2.6	2.0	2.3	3.5	14	-1.5
75S(66)	0.1	6.0	37.7	6.5	37.0	-8	0.7
	0.2	10.2	22.9	8.8	21.9	16	1.0
	0.5	10.0	13.2	10.3	12.1	-3	1.1
	1.0	9.7	10.2	11.3	10.5	-14	-0.3
	2.0	8.1	7.0	7.6	5.1	7	1.9
	4.0	6.4	4.7	5.0	3.5	29	1.2

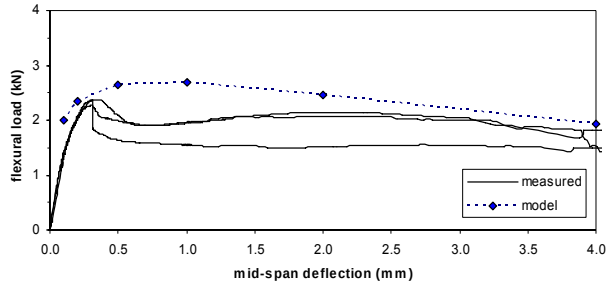

Fig. 10 - Comparison between predicted and measured response – 50 x 100 mm cast beam, 40 kg/m^3 (inferred fibre pull-out response).

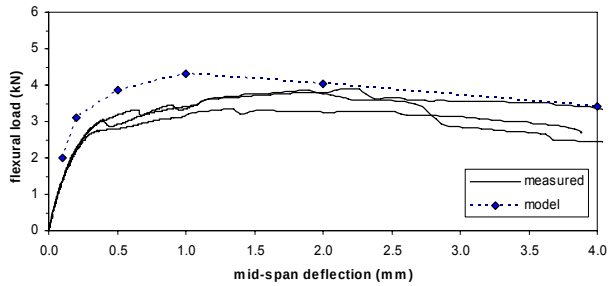

Fig. 11 - Comparison between predicted and measured response – 50 x 100 mm cast beam, 80 kg/m^3 (inferred fibre pull-out response).

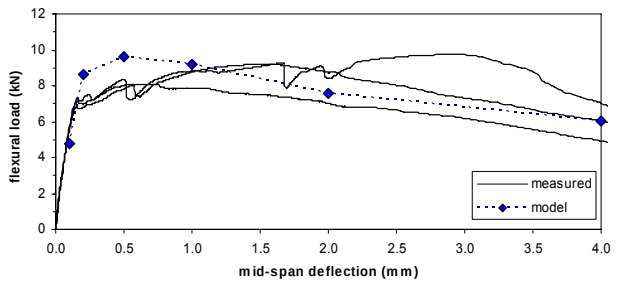

Fig. 12 - Comparison between predicted and measured response – 75 x 100 mm cast beam, 80 kg/m^3 (inferred fibre pull-out response).

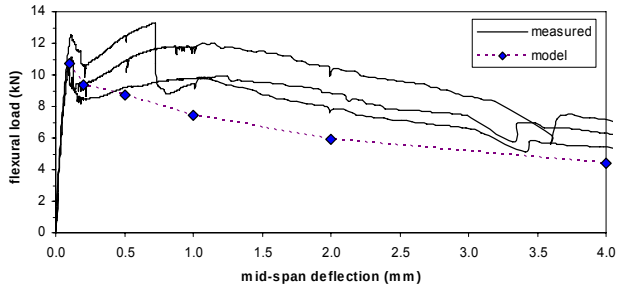

Fig. 13 - Comparison between predicted and measured response – 100 x 100 mm cast beam, 40 kg/m^3 (inferred fibre pull-out response).

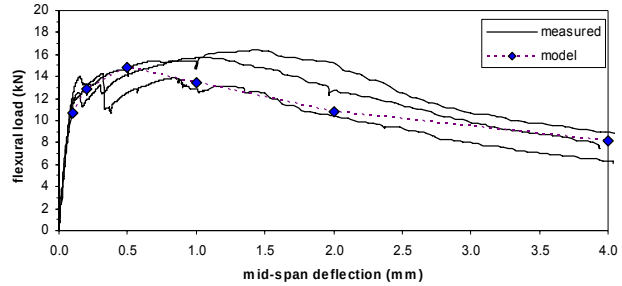

Fig. 14 - Comparison between predicted and measured response – 100 x 100 mm cast beam, 80 kg/m^3 (inferred fibre pull-out response).

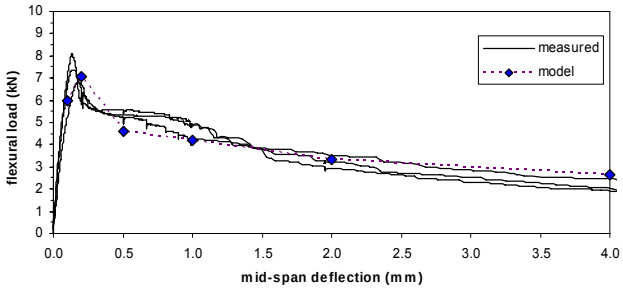

Fig. 15 - Comparison between predicted and measured response – 75 x 125 mm sprayed beam, 26 kg/m^3 (inferred fibre pull-out response).

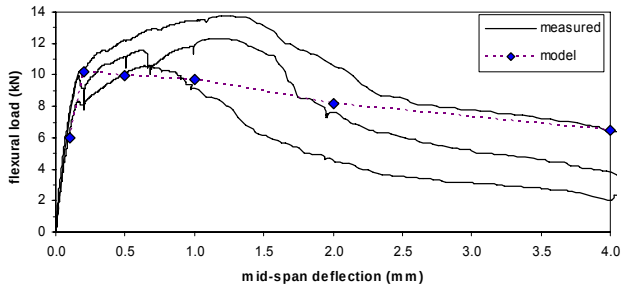

Fig. 16 - Comparison between predicted and measured response – 75 x 125 mm sprayed beam, 66 kg/m^3 (inferred fibre pull-out response).